Science & Technology Development Journal 2022, 25(2):2424-2431

Open Access Full Text Article

Research Article

Synthesis of TeO_2 nanoparticles by tellurium oxidation in NH_4OH and their infrared sensing properties

Dang Duc Vuong, Vu Xuan Hien*

ABSTRACT

Tellurium oxide is an interesting semiconductor metal oxide with a variety of fascinating photoelectric properties. The method of thermal oxidation of tellurium metal in air was used to make TeO_2 nanowires and rods. This paper introduces a facile method to synthesize TeO_2 nanoparticles directly from tellurium powder in NH_4OH solution. The TeO_2 nanoparticles are monodisperse, uniform and high density. The growth mechanism of the TeO_2 nanoparticles was proposed and debated. This material has a good ability to absorb infrared light with a wavelength of 800 nm. The infrared photosensing properties of this nanomaterial were investigated and compared to those of recent studies.

Key words: Nanoparticles, light sensors, metal oxides, tellurium

INTRODUCTION

Tellurium is a rare metal that can be found in the Earth's crust. Tellurium monoxide (TeO), tellurium dioxide (TeO_2), and tellurium trioxide (TeO_3) are the most common oxides of this metal. TeO is gray in color when powdered in dry air. This compound is typically unstable, easily oxidizing to Te and TeO_2 in dry air and humidity at high temperatures, respectively [1]. TeO_2 is the most stable tellurium oxide out of all of them. Due to its outstanding optical properties, this p-type semiconductor (Eg of 3.3-3.8 eV) is being researched and used in a variety of fields, including memory switching devices [2], optical storage materials [3], amplifiers and integrated optics [4], laser devices [5], catalysts [6], and ensor [7–9]. With many interesting applications, TeO_2 nanomaterials have been synthesized by various physical and chemical methods [10–12]. Recently, several research groups have successfully synthesized TeO_2 nanorods directly from tellurium metal by thermal oxidation [13–15]. This is a simple method that allows the synthesis of nanomaterials directly on metal surfaces with high density and uniformity [16]. However, this method requires an elevated temperature (above 300 °C) and cannot control the morphology of the postsynthesized material [16]. Recently, metal oxidation in alkaline solution was applied by several groups in the syntheses of metal oxide nanostructures [17–19]. By a similar method, our research group successfully synthesized CuO, $Ni(OH)_2$ and V_2O_5 nanoplates or nanosheets [20–22]. To date, there have been no studies on the synthesis of TeO_2 nanomaterials by tellurium oxidation in alkaline solution.

In this study, we proposed a facile process based on tellurium oxidation in NH_4OH solution to synthesize highly uniform TeO_2 nanomaterials. The morphology and structure of the synthesized nanomaterials were characterized by scanning electron microscopy (SEM), X-ray diffraction (XRD), ultraviolet–visible spectroscopy (UV–Vis), and energy-dispersive X-ray spectroscopy (EDS). For application, the optical sensing properties of the as-synthesized nanomaterials were investigated using several light sources (wavelengths of 450 nm, 600 nm, and 800 nm). Interestingly, the TeO_2 nanoparticles showed resistance fluctuation under exposure to the light source. The e result were compared to those of other photosensitive materials with similar electrode structures.

MATERIALS-METHODS

Figure 1 depicts the TeO_2 nanoparticle fabrication process, which is broken down into simple steps. First, a heat-resistant 100 ml Duran vial was filled with 0.2 g of tellurium powder (99.99 % purity, Sanno Co., China) and 20 ml of NH_4OH solution (25 %, w/v, Xilong Scientific Co., China). After that, the solution mixture was kept in an oven for 24 h at 80 °C. The vial of solution was allowed to cool naturally to room temperature after the heat treatment was completed. The final product was a white powder that had been filtered and washed with deionized water three times. The powder sample is coated on a glass substrate after fabrication. After drying, scanning electron microscopy (SEM, Hitachi tabletop Microscopes

School of Engineering Physics, Hanoi University of Science and Technology, No. 01 Dai Co Viet, Hai Ba Trung, Hanoi

Correspondence

Vu Xuan Hien, School of Engineering Physics, Hanoi University of Science and Technology, No. 01 Dai Co Viet, Hai Ba Trung, Hanoi

Email: hien.vuxuan@hust.edu.vn

History

- Received: 2022-01-15
- Accepted: 2022-06-06
- Published: 2022-06-30

DOI : 10.32508/stdj.v25i2.3887

Cite this article : Vuong D D, Hien V X. **Synthesis of TeO_2 nanoparticles by tellurium oxidation in NH_4OH and their infrared sensing properties**. *Sci. Tech. Dev. J.;* 25(2):2424-2430.

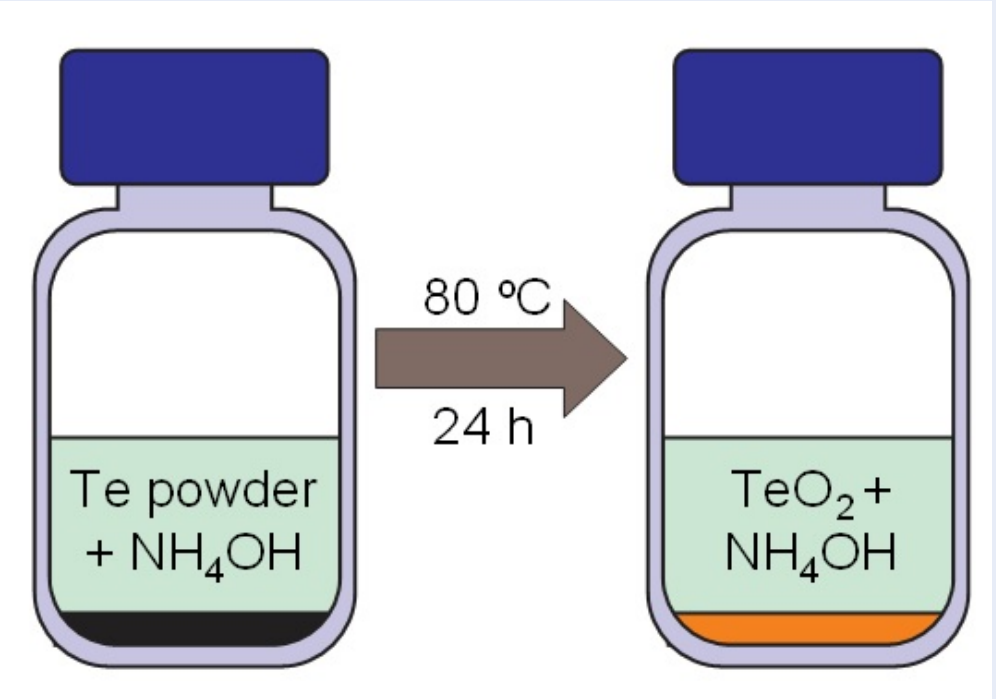

Figure 1: **Synthesis process of TeO_2 nanoparticles from tellurium powder.** The precursors of 0.2 g Te powder and 20 ml NH_4OH aqueous solution were heated at 80 °C for 24 h to make TeO_2 nanoparticles.

TM4000Plus, Hitachi Co., Japan) and energy dispersive X-ray spectroscopy (EDS) were used to examine the surface morphology and elemental composition of this powder sample. X-ray diffraction (XRD, X'Pert-Pro, Malvern Panalytical Ltd., United Kingdom) was used to investigate the crystal structures of the postfabricated powder samples. The optical properties and chemical compositions were investigated using an ultraviolet–visible spectrophotometer (UV–Vis; JASCO V-750, Jasco, Japan). The Tauc method is used to determine the width of the optical band gap of the material[23]:

$$ahv = B\left(hv - E_g\right)^n \quad (1)$$

where α, $h\upsilon$, B, E_g, and n are the optical absorption coefficient, incident photon energy, constant, optical energy gap, and exponent corresponding to the type of optical transition (direct allowed: n = 0.5, direct forbidden: n = 1.5, indirect allowed: n = 2, indirect forbidden: n = 3), respectively[24].

To investigate the material's photosensitive properties, TeO_2 nanoparticles were coated on a Pt interdigitated electrode (Figure 2a). The following are the small steps in the coating process. First, ultrasonic vibration was used to disperse 0.05 g of the prefabricated powder sample in 5 mL of distilled water. Then, using a micropipette, 20 L of this solution mixture was dripped onto the electrode surface. The electrode was then dried at 60 °C for 12 h. Figure 2b depicts the structure of our homemade photosensing measurement system. After coating, the electrode was placed on a hot plate.

$$S = \frac{I_{ph}}{I_{dark}} \quad (2)$$

The light response is determined by the ratio of the current flowing through the device under illumination (I_{ph}) to the current flowing through the device in the dark (I_{dark}). The device is powered by a DC voltage of 1 V. The rise time is defined as 90 % of the time the measuring circuit switches from dark to bright. When the measuring circuit turns from light to dark, the decay time is 90 % of the switching time.

RESULTS

The morphology and dimensions of the synthesized sample are shown in Figure 3. This sample is made up of monodispersed nanoparticles. The particle size distribution graph in Figure 3b indicates that the particle sizes are distributed in the range of 15 to 250 nm. The Lorentz distribution revealed that particles with a diameter of 85 nm made up the majority of the

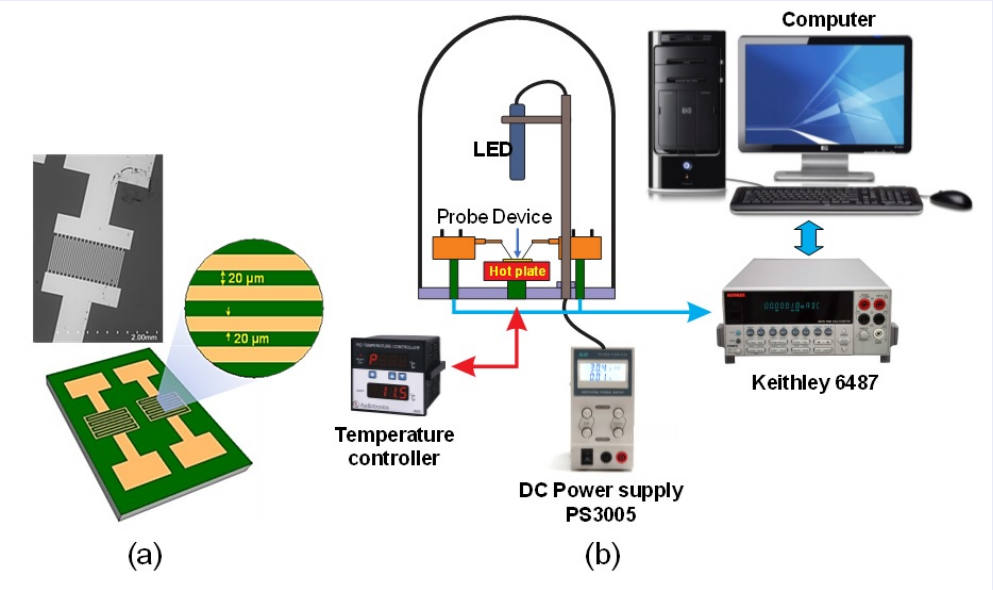

Figure 2: **Model of the electrode structure and measuring system.** (a) Structure and SEM images of the interdigitated electrode and (b) our homemade photosensing measurement system. The interdigitated electrode was patterned by photolithography with an electrode gap of 20 μm. The measurement system contains a temperature controller to regulate the hotplate temperature. After being fixed by two probes, the current flowing through the electrode coated with TeO_2 nanoparticles can be measured by a Keithley 6487. An application is made by LabVIEW to connect the Keithley device and a computer. The DC source DS3005 is used to power the LEDs.

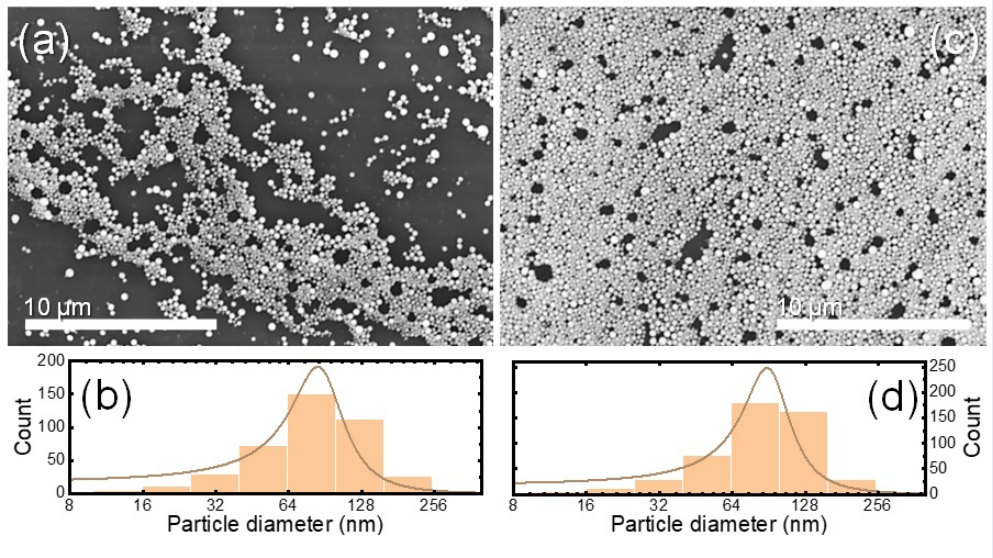

Figure 3: **Shape and dimensions of the synthesized nano materials.** (a, c) SEM image of the as-synthesized samples and (b, d) corresponding particle size distribution at different locations. The synthesized white powder was distributed onto carbon tape for SEM observation. Particle analysis was carried out using the ImageJ application.

particles in this sample. The particle size distribution graph (Figure 3d), which is based on an SEM image of a different area (Figure 3c), yields similar results to the previously analyzed data.

Because no diffraction peak is found in the XRD pattern in Figure 4a, the fabricated sample may exist in an amorphous state. As a result, it is suggested that the synthesized nanoparticles may be constructed by isotropic aggregation. Nevertheless, the chemical composition of this sample cannot be determined or predicted. Therefore, the UV–Vis method is used to characterize the samples. ased on the strong upward curvature of the UV–Vis absorption spectrum in Figure 4b, high absorption at a wavelength of nearly 800 nm of the fabricated sample is observed. The Tauc plot in Figure 4c indicates the material's optical bandgap of 1.57 eV by intersecting the tangent of this curve with the horizontal axis at y = 0. This bandgap value is predicted to be consistent with the TeO_2 material, as previously announced by I. A. Kariper, using Te metal powder and NH_4OH solution as a precursor[25]. EDS analysis of the synthesized powder sample was further used to confirm the existence of TeO_2.

Figure 5a depicts the analyzed sample area. The EDS analysis in Figure 5b shows that the sample contains two elements, Te and O. The Te:O atom ratio is 31:69, which corresponds to the appearance of the TeO_2 composition. Figure 5c and Figure 5d show mapping images of the Te and O element , respectively. The distribution of the bright and dark areas on these images is quite uniform, showing that the TeO_2 nanoparticles are well formed.

The photosensing properties of the TeO_2 nanoparticles tested with several LEDs are shown in Figure 6. The sensor response toward several wavelengths of 450, 600, and 800 nm is shown in Figure 6a. In these data, the device demonstrates the highest response to an 800 nm LED (I_{ph}/I_{dark} of 17), which is 12 times higher than that to a 450 nm LED and 15 times higher than the response to a 600 nm LED. The rise (Figure 6b) and decay (Figure 6c) curves are magnified along the time axis, revealing that the 800 nm device's rise versus decay times are 90 ms and 270 ms, respectively. When compared to other sensing nanomaterials with similar electrode structures, these rise and decay times are quite impressive (Table 1). The device's modulation toward seven light pulses is shown in Figure 6d. The sensor's response versus rise/decay time through seven signal pulses is identical. This result demonstrates that the TeO_2 nanoparticle-based sensor performs quite stably under the test conditions.

DISCUSSION

The formation of the TeO_2 composition after treating Te powder in NH_4OH can be understood by the oxidation of metal in an alkaline medium, which is proposed elsewhere[30]. In this experiment, the formation process of the TeO_2 nanoparticles can be described as follows. First, metallic Te powder reacts with NH_4OH solution to form a complex $[Te(NH_3)_6]^{2+}$:

$$Te + O_2 + H_2O + NH_3 \rightarrow [Te(NH_3)_6]^{2+} \quad (3)$$

In alkaline solution, OH^- ions can replace NH_3 in this complex to form a tellurium hydroxide[17,31]:

$$[Te(NH_3)_6]^{2+} + OH^- \rightarrow Te(OH)_4 \quad (4)$$

Then, $Te(OH)_4$ can be converted to TeO_2 by the following reaction:

$$Te(OH)_4 \rightarrow TeO_2 + 2H_2O \quad (5)$$

Thus, tellurium metal powder can be completely oxidized to TeO_2 in an NH_4OH solution. The formed TeO_2 molecules can be separated from the tellurium surface and move freely in the solution due to the thermal energy. The series of reactions according to equations (3), (4), and (5) continues until all the tellurium is oxidized to TeO_2. In addition, thermal oscillations of TeO_2 molecules in solution can lead to anisotropic aggregation forming spherical nanoparticles. According to our predictions, the size of these TeO_2 nanoparticles could be controlled by solution temperature, sample treatment time, or solution volume. Studying the effect of these parameters on the size and shape of TeO_2 nanoparticles should be carried out in another study.

The device acts as a photoconductor since its structure is TeO_2 nanoparticles coated on an interdigitated electrode. The increase in I_{ph} under illumination may be related to the increase in the number of carriers in the TeO_2 semiconductor. Indeed, the energy of incident light may excite band-to-band transitions of electrons, forming electron-hole pairs[32]:

$$h\nu \rightarrow h^+ + e^- \quad (6)$$

These generated electron-hole pairs can travel in reverse directions when an external electric field is applied to the device. As a result, the electrical current flowing through the device increases[33]. Based on the adsorption spectrum of TeO_2 nanoparticles in Figure 4b, this material best absorbs infrared light (wavelength of 800 nm). This is quite consistent with the photosensitive results shown in Figure 6a. Although more investigations are expected to evaluate the photosensing properties of the synthesized TeO_2 nanoparticles, the fast response of this nanomaterial to infrared light suggests potential for practical application.

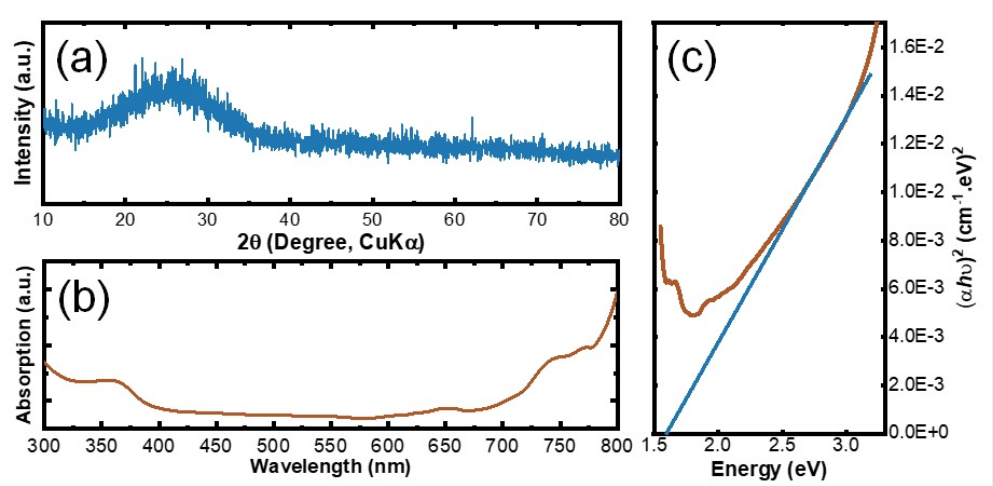

Figure 4: **Crystal structure and optical properties of the synthesized nano materials.** (a) X-ray diffraction pattern, (b) UV–Vis absorption spectrum and (c) Tauc plot of the synthesized sample.

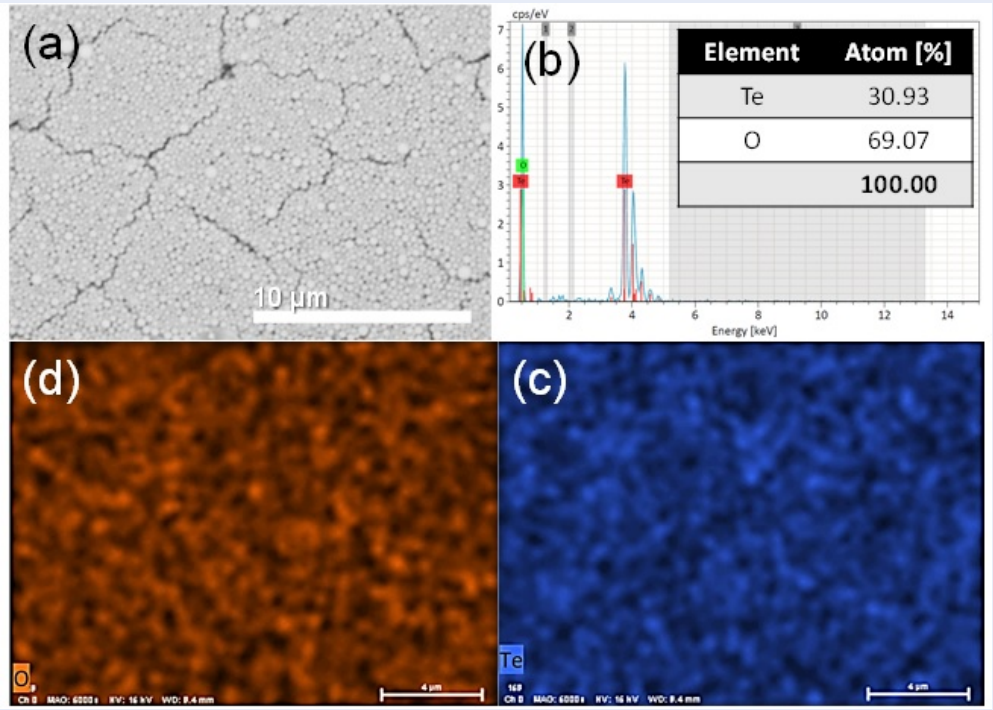

Figure 5: **Analysis of elemental composition in synthesized nanomaterials.** (a) SEM image, (b) EDS spectrum, distribution mapping image of (c) Te and (d) O atoms in the analysis area.

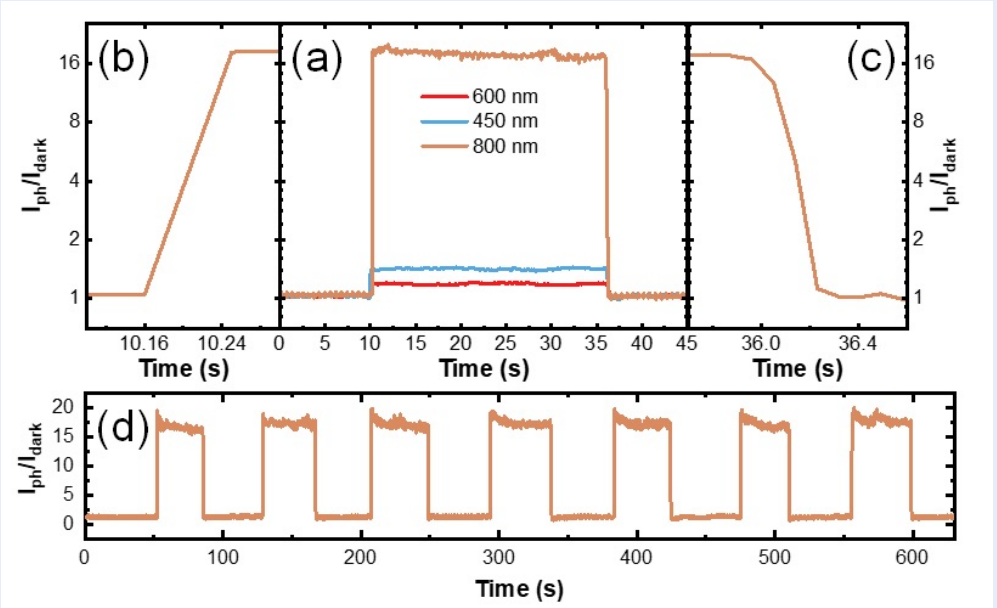

Figure 6: **Photoresponse characteristics of the TeO_2 nanoparticles.** (a) Time-dependent photoresponse of the TeO_2 nanoparticles illuminated by 450, 600, and 800 nm LEDs, (b) rise and (c) decay curves of the TeO_2 nanoparticles under 800 nm light. (d) Modulation of the photoresponse versus measured time under 7 light pulses (800 nm).

Table 1: Comparison table of the rise and decay times of several photosensitive nanomaterials.

Nanomaterials	Response time (ms)	Recovery time (ms)	Ref.
Graphene oxide/carbon nanoparticles thin film	~ 5000	~2000	[26]
Gaphene/Ti_2O_3 nanoparticles	~ 3	~ 10	[27]
ZnO nano film with Au nanoparticles	~300000	~300000	[28]
ZnO nanoparticles	~60000	~500000	[29]
TeO_2 nanoparticles	90	270	This work

CONCLUSIONS

Monodispered TeO_2 nanoparticles with an average diameter of 85 nm were synthesized by oxidation of Te powder in an NH_4OH solution at 80 °C for 24 h. The synthesized nanomaterial was amorphous with an optical bandgap of 1.57 eV. The formation process of the TeO_2 nanoparticles was proposed and discussed. Since the synthesized TeO_2 nanoparticles can strongly absorb infrared light, their photosensing properties were investigated using several LEDs with wavelengths of 450, 600, and 800 nm. The TeO_2 nanoparticles showed the highest response of 17. The rise versus decay times were 90 and 270 ms, respectively. With a simple synthesis process, the fast response of the TeO_2 nanoparticles to infrared radiation has potential for practical application.

LIST OF ABBREVIATIONS

SEM: scanning electron microscopy

EDS: energy dispersive X-ray spectroscopy

XRD: X-ray diffraction

UV–Vis: ultraviolet–visible spectrophotometer

LED: light-emitting diode

COMPETING INTERESTS

The authors declare that they have no competing interests.

AUTHORS' CONTRIBUTIONS

All authors equally contributed to this work, read and approved the final vesion for publication.

ACKNOWLEDGMENTS

This research is funded by the Vietnam National Foundation for Science and Technology Development (NAFOSTED) under Grant 103.02-2019.25.

REFERENCES

1. Greenwood. Chemistry of Elements. Sykepleien 1968; 55: 735-736;Available from: https://doi.org/10.1016/S0016-5085(19)33978-2.
2. Tirupataiah C, Narendrudu T, Suresh S, Srinivasa Rao P, Vinaya Teja PM, Sambasiva Rao M V. et al. Influence of valence state of copper ions on structural and spectroscopic properties of multi-component PbO-Al2O2-TeO2-GeO2-SiO2 glass ceramic system- a possible material for memory switching devices. Opt Mater (Amst) 2017; 73: 7-15;Available from: https://doi.org/10.1016/j.optmat.2017.07.040.
3. Hodgson SNB, Weng L. Sol-Gel Processing of Tellurium Oxide and Suboxide Thin Films with Potential for Optical Data Storage Application. J Sol-Gel Sci Technol 2000 182 2000; 18: 145-158;Available from: https://doi.org/10.1023/A:1008717003930.
4. Shen S, Jha A, Liu X, Naftaly M, Bindra K, Bookey HJ et al. Tellurite Glasses for Broadband Amplifiers and Integrated Optics. J Am Ceram Soc 2002; 85: 1391-1395;Available from: https://doi.org/10.1111/j.1151-2916.2002.tb00286.x.
5. Jha A, Richards B, Jose G, Teddy-Fernandez T, Joshi P, Jiang X et al. Rare-earth ion doped TeO2 and GeO2 glasses as laser materials. Prog Mater Sci 2012; 57: 1426-1491;Available from: https://doi.org/10.1016/j.pmatsci.2012.04.003.
6. Castellan A, Vaghi A, Bart JCJ, Giordano N. Propylene oxidation on TeO2·SiO2 catalysts. J Catal 1975; 39: 213-224;Available from: https://doi.org/10.1016/0021-9517(75)90326-7.
7. Rai VK, Rai DK, Rai SB. Pr3+ doped lithium tellurite glass as a temperature sensor. Sensors Actuators A Phys 2006; 128: 14-17;Available from: https://doi.org/10.1016/j.sna.2005.12.030.
8. Dewan N, Sreenivas K, Gupta V. Comparative study on TeO2 and TeO3 thin film for γ-ray sensor application. Sensors Actuators A Phys 2008; 147: 115-120;Available from: https://doi.org/10.1016/j.sna.2008.04.011.
9. Wu Y, Hu M, Qin Y, Wei X, Ma S, Yan D. Enhanced response characteristics of p-porous silicon (substrate)/p-TeO2 (nanowires) sensor for NO2 detection. Sensors Actuators B Chem 2014; 195: 181-188;Available from: https://doi.org/10.1016/j.snb.2014.01.019.
10. Qin B, Bai Y, Zhou Y, Liu J, Xie X, Zheng W. Structure and characterization of TeO2 nanoparticles prepared in acid medium. Mater Lett 2009; 63: 1949-1951;Available from: https://doi.org/10.1016/j.matlet.2009.06.018.
11. Hongwang Z, Swihart MT. Synthesis of Tellurium Dioxide Nanoparticles by Spray Pyrolysis. Chem Mater 2007; 19: 1290-1301;Available from: https://doi.org/10.1021/cm062257n.
12. Cho SC, Hong YC, Uhm HS. TeO2 nanoparticles synthesized by evaporation of tellurium in atmospheric microwave-plasma torch-flame. Chem Phys Lett 2006; 429: 214-218;Available from: https://doi.org/10.1016/j.cplett.2006.08.026.
13. Choi MS, Bang JH, Mirzaei A, Na HG, Jin C, Oum W et al. Exploration of the use of p-TeO2-branch/n-SnO2 core nanowires nanocomposites for gas sensing. Appl Surf Sci 2019; 484: 1102-1110;Available from: https://doi.org/10.1016/j.apsusc.2019.04.122.
14. Filippo E, Micocci G, Tepore A, Siciliano T. Fabrication of α-TeO2 smooth and beaded microwires by thermal evaporation method. J Cryst Growth 2011; 336: 101-105;Available from: https://doi.org/10.1016/j.jcrysgro.2011.09.047.
15. Liu Z, Yamazaki T, Shen Y, Kikuta T, Nakatani N. Synthesis and characterization of TeO2 nanowires. Jpn J Appl Phys 2008; 47: 771-774;Available from: https://doi.org/10.1143/JJAP.47.771.
16. Zhu Y, Sow CH. Hotplate technique for nanomaterials. Cosmos 2008; 04: 235-255;Available from: https://doi.org/10.1142/S0219607708000354.
17. Soejima T, Yagyu H, Kimizuka N, Ito S. One-pot alkaline vapor oxidation synthesis and electrocatalytic activity towards glucose oxidation of CuO nanobelt arrays. RSC Adv 2011; 1: 187-190;Available from: https://doi.org/10.1039/c1ra00109d.
18. Kaur G, Saini K, Tripathi AK, Jain V, Deva D, Lahiri I. Room temperature growth and field emission characteristics of CuO nanostructures. Vacuum 2017; 139: 136-142;Available from: https://doi.org/10.1016/j.vacuum.2017.02.020.
19. Soejima T, Takada K, Ito S. Alkaline vapor oxidation synthesis and electrocatalytic activity toward glucose oxidation of CuO/ZnO composite nanoarrays. Appl Surf Sci 2013; 277: 192-200;Available from: https://doi.org/10.1016/j.apsusc.2013.04.024.
20. Hien VX, Minh NH, Son DT, Nghi NT, Phuoc LH, Khoa CT et al. Acetone sensing properties of CuO nanowalls synthesized via oxidation of Cu foil in aqueous NH4OH. Vacuum 2018; 150: 129-135;Available from: https://doi.org/10.1016/j.vacuum.2018.01.030.
21. Hien VX, Vuong DD, Chien ND, Heo Y-W. Shape-controlled synthesis of Ni(OH)2/NiO nanowalls by surface reaction of Ni foil in aqueous NH4OH. Mater Chem Phys 2018; 217: 74-81;Available from: https://doi.org/10.1016/j.matchemphys.2018.06.054.
22. Hien VX, Nhat DD, Nghi NT, Phuoc LH, Khoa CT, Vuong DD et al. From vanadium powder to vanadium pentoxide rolled-up nanosheets: Hydrothermal synthesis and its ethanol sensing properties. Mater Sci Semicond Process 2021; 126;Available from: https://doi.org/10.1016/j.mssp.2021.105670.
23. Beke S, Giorgio S, Korösi L, Nánai L, Marine W. Structural and optical properties of pulsed laser deposited V2O5 thin films. Thin Solid Films 2008; 516: 4659-4664;Available from: https://doi.org/10.1016/j.tsf.2007.08.113.
24. Ramana C V., Hussain OM, Uthanna S, Naidu BS. Influence of oxygen partial pressure on the optical properties of electron beam evaporated vanadium pentoxide thin films. Opt Mater (Amst) 1998; 10: 101-107;Available from: https://doi.org/10.1016/S0925-3467(97)00168-7.
25. Kariper IA. Optical properties and surface energy of tellurium oxide thin film. J Opt 2018 474 2018; 47: 504-510;Available from: https://doi.org/10.1007/s12596-018-0485-7.
26. Chowdhury FA, Hossain MA, Uchida K, Tamura T, Sugawa K, Mochida T et al. Graphene oxide/carbon nanoparticle thin film based IR detector: Surface properties and device characterization. AIP Adv 2015; 5: 107228;Available from: https://doi.org/10.1063/1.4935042.
27. Yu X, Li Y, Hu X, Zhang D, Tao Y, Liu Z et al. Narrow bandgap oxide nanoparticles coupled with graphene for high performance mid-infrared photodetection. Nat Commun 2018 91 2018; 9: 1-8;PMID: 30327474. Available from: https://doi.org/10.1038/s41467-018-06776-z.
28. Chinh ND, Hien TT, Do Van L, Hieu NM, Quang ND, Lee SM et al. Adsorption/desorption kinetics of nitric oxide on zinc oxide nano film sensor enhanced by light irradiation and gold-nanoparticles decoration. Sensors Actuators B Chem 2019; 281: 262-272;Available from: https://doi.org/10.1016/j.snb.2018.10.113.
29. Chang SP, Chen KJ. Zinc oxide nanoparticle photodetector. J Nanomater 2012; 2012;Available from: https://doi.org/10.1155/2012/602398.
30. Anandan S, Wen X, Yang S. Room temperature growth of CuO nanorod arrays on copper and their application as a cathode in dye-sensitized solar cells. Mater Chem Phys 2005; 93: 35-40;Available from: https://doi.org/10.1016/j.matchemphys.2005.02.002.
31. Kaur G, Saini K, Tripathi AK, Jain V, Deva D, Lahiri I. Room temperature growth and field emission characteristics of CuO nanostructures. Vacuum 2017; 139: 136-142;Available from: https://doi.org/10.1016/j.vacuum.2017.02.020.
32. Simon M. Sze M-KL. Semiconductor Devices: Physics and Technology. Wiley, 2012;.
33. Yan Y, Liu Q, Du X, Qian J, Mao H, Wang K. Visible light photoelectrochemical sensor for ultrasensitive determination of

dopamine based on synergistic effect of graphene quantum dots and TiO2 nanoparticles. Anal Chim Acta 2015; 853: 258-264;PMID: 25467467. Available from: https://doi.org/10.1016/j.aca.2014.10.021.